Mechanics of evolutionary digit reduction in fossil horses (Equidae)

Mechanics of evolutionary digit reduction in fossil horses (Equidae)

Brianna K. McHorse*[1,2], Andrew A. Biewener[2], Stephanie E. Pierce[1]

1 Museum of Comparative Zoology and Department of Organismic and Evolutionary Biology, Harvard University, Cambridge, MA 02138, USA

2 Concord Field Station, Department of Organismic and Evolutionary Biology, Harvard University, Bedford, MA 01730, USA

* Email: bmchorse@fas.harvard.edu

Abstract

Digit reduction is a major trend that characterizes horse evolution, but its causes and consequences have rarely been quantitatively tested. Using beam analysis on fossilized centre metapodials, we tested how locomotor bone stresses changed with digit reduction and increasing body size across the horse lineage. Internal bone geometry was captured from 13 fossil horse genera that covered the breadth of the equid phylogeny and the spectrum of digit reduction and body sizes, from *Hyracotherium* to *Equus*. To account for the load-bearing role of side digits, a novel, continuous measure of digit reduction was also established – Toe Reduction Index (TRI). Our results show that without accounting for side digits, three-toed horses as late as *Parahippus* would have experienced physiologically untenable bone stresses. Conversely, when side digits are modelled as load-bearing, species at the base of the horse radiation through *Equus* likely maintained a similar safety factor to fracture stress. We conclude that the centre metapodial compensated for evolutionary digit reduction and body mass increases by becoming more resistant to bending through substantial positive allometry in internal geometry. These results lend support to two historical hypotheses: that increasing body mass selected for a single, robust metapodial rather than several smaller ones; and that, as horse limbs became elongated, the cost of inertia from the side toes outweighed their utility for stabilization or load-bearing.

Keywords

digit reduction, locomotion, biomechanics, beam bending, evolution

Introduction

Digit reduction and loss is a repeated theme in tetrapod evolution, in groups as disparate as theropod dinosaurs, lizards, marsupials, rodents, and ungulates [1–6]. Reduction from the ancestral state of five digits, or more in Devonian tetrapods [7], contributes to the remarkable diversity of limb form and function in living tetrapods. Evolutionary digit reduction requires interaction between development and selective pressures that drive adaptation. The developmental mode of digit reduction varies, even within mammalian orders [8,9], and the selective pressures that interact with these developmental changes are often associated with new ecological behaviours and locomotor modes [4,10,11]. In dipodid rodents, for example, repeated convergent evolution of reduced digits suggests selection for increased bipedality, with a concomitant shift to rapid, unpredictable locomotion for predator evasion [4,12].

One of the most extreme examples of digit reduction is the modern horse (genus *Equus*), which evolved monodactyly (a single toe) from an ancestral state of four digits in front and three behind [13]. All phalanges other than digit III are eliminated, and metapodials II and IV are vestigial "splint" bones that taper off halfway down the length of metapodial III. In horses, the classic explanation for digit reduction is that of an adaptive response to the replacement of forests by grasslands, although the specific underlying driver for monodactyly has been debated. Shifting to hard turf and open spaces is suggested to select for long, slender legs to: increase speed for predator escape [14]; decrease the energetic cost of locomotion by reducing distal limb mass [15]; or enhance stability for high-speed, straight-lined movements [16]. An additional hypothesis proposed for digit reduction in the horse lineage is that evolutionary increases in body mass produced greater bending forces on the limbs and a single digit resists bending forces better than several smaller digits of the same total size [17,18]. We aim to test the body mass

hypothesis by exploring how locomotion-related stresses in the metapodials change with the evolution of larger body sizes and reduced side digits.

Prior work on equid limb evolution has focused on the transition from digitigrade to unguligrade posture, generally using *Mesohippus* (tridactyl with large side digits), *Merychippus* (tridactyl with reduced side digits), and *Equus* (monodactyl) as exemplars for key stages of digit reduction. Using inferences from tendon scars and articular surfaces, *Mesohippus* has been reconstructed as subunguligrade with a digital pad that helps absorb forces, while *Merychippus* has been reconstructed as unguligrade with non-functional side digits (similar to *Equus*) [17,19,20]. These studies assume that as the foot becomes more upright and the central phalanges elongate, the side digits lose function. A mechanical investigation of digit reduction estimated bending forces on the third metacarpal in all three taxa [21]. Using external measurements and cross-sections (estimated from fractured specimens), mid-shaft bending stresses were calculated to be within the range found by in vivo experiments on mammals. Forces for *Mesohippus* were reduced by 50%, assuming that each side digit carried 25% of the load, but the side digits of *Merychippus* were assumed to play no functional role [21]. The only other test of load-bearing in side digits comes from a *Hipparion* trackway that shows contact from the side digits, supporting possible load-bearing or stabilizing functions [22].

Here we significantly expand the beam bending approach by using modern 3D imaging to capture the internal bone geometry of metapodial III from 13 fossil horse genera. The taxa in this study cover the breadth of the equid phylogeny and the full spectrum of body sizes and digit reduction, from the dog-sized, tetra/tridactyl *Hyracotherium* to the large, monodactyl *Equus*. Unlike prior studies, we also quantitatively account for the changing size of side digits through

evolutionary time by scaling ground reaction forces relative to a continuous measure of digit state. Our study addresses the following three questions and associated hypotheses:

(1) How does stress on the centre metapodial change with evolutionary increases in body size? As quadrupeds tend to maintain similar long bone safety factors regardless of size [23,24], we hypothesized maximal metapodial III stresses to remain constant through evolution by adjusting its cross-sectional geometry to increase resistance to bending.

(2) Did side digits play a load-bearing role during horse evolution? If load is placed entirely on the centre metapodial, we hypothesized stress on metacarpal III to be high in species with load-bearing side digits and within normal ranges for species with non-load-bearing side digits. Likewise, if side digits share the load proportional to their size, we hypothesized stress on the centre metapodial to remain constant through evolution.

(3) Is the geometry of metacarpal III better or worse at withstanding bending forces than metatarsal III? In extant horses, the metatarsal experiences slightly higher bending forces than the metacarpal because it is less closely aligned to the ground reaction force [25,26]. Because the equid hind limb shows reduced digits earlier than the forelimb, we hypothesized a more rapid increase in bending strength of metatarsal III relative to metacarpal III.

Material and Methods

(a) Specimens and internal geometry

This study uses metapodials (n = 26) from 13 fossil horse genera and *Tapirus bairdii* (Figure 1; electronic supplementary material, methods and table S1). Tapirs are the most relevant comparative outgroup, as they are the only extant perissodactyls with similar distal limb morphology to early horses (but see [27] for discussion of varying morphology and locomotor

styles within the genus). All specimens were micro-CT scanned using a Nikon Metrology (X-Tek) HMXST225 MicroCT system, reconstructed as a downsampled TIFF stack, and processed using the Bone Geometry function of the BoneJ (v1.0.0) plugin for ImageJ (v1.48v) [28,29]. In addition to bone length (l), we extracted from every slice the cross-sectional area (A), second moment of area about the mediolateral (I_{ML}, bending in the anteroposterior direction) and anteroposterior (I_{AP}, bending in the mediolateral plane) axes, and radius from the neutral axis in both directions (y_{AP}, y_{ML}; Figure S1). The mid-shaft slice of each specimen was then used for bending analysis (see below); if the exact midshaft slice was damaged or otherwise unsuitable, we chose the nearest suitable slice.

We tested the scaling of evolutionary changes in midshaft cross-sectional area (a measure of bone compressive strength) and second moment of area (a measure of resistance to bending). To correct for the effect of phylogeny, we calculated independent contrasts on log-transformed mass and internal geometry variables [30]. Using major axis regression in the R package smatr [31], we then tested whether the slopes of the mass vs. internal geometry contrasts were significantly different from isometry (defined as a slope of 2/3 for cross-sectional area and 4/3 for second moment of area). Cross-sectional area and second moment of area were also plotted along the length of the bone, with genera coloured according to digit state, to assess how internal geometry changes with reduction in digits. For this comparison, second moment of area (I_{AP} and I_{ML}, mm^4) was size-corrected by taking the 4th root to provide a size-independent measure of shape, while retaining the evolutionary signal of increasing bone length [32]. Similarly, cross-sectional area (A, mm^2) was corrected by taking the square root.

(b) Loading scenarios and conditions

122 To estimate bone stress, we simulated two loading scenarios: normal, steady-state
123 forward locomotion (approximately trotting speed) and high-performance forward locomotion
124 (rapid acceleration or jumping). Based on in vivo locomotion data on modern horses [25,26], the
125 angle of each metapodial relative to the ground reaction force was set to 5° and 20°, respectively,
126 for these two loading scenarios. For each loading scenario, either (i) a full body-weight load was
127 applied to the centre metapodial (digit III) using reconstructed body mass values [33–36],
128 matching the ground reaction force that medium-sized animals experience at a trotting gait,
129 including extant horses [25,26,37]; or (ii) the body-weight load applied to metapodial III was
130 reduced relative to the side digits bearing some of the load. The relative body-weight load
131 applied to metapodial III was determined by a Toe Reduction Index (TRI; see electronic
132 supplementary methods and table S2). TRI is a ratio of side digit length to centre digit length in
133 the proximal phalanx. The ratio ranges from 0, where no side toes are present (e.g. *Equus*) to 1,
134 where all digits are of equal size (Figure 1), using the simplifying assumption that load capacity
135 correlates directly with digit size. For example, a TRI of 0 (e.g., *Equus*) produces a scaled load
136 equal to the full body weight, whereas a TRI of 1 (all three digits equal in size) produces a scaled
137 load of 1/3 body weight.
138
139 (d) Beam bending
140 Using beam mechanics, we estimated the stress at the metapodial midshaft (Figure S1). We
141 calculated bending in the anteroposterior direction, simulating forward locomotion, by
142 combining stress from axial compression:
143

144 $$\sigma_c = -\frac{F_m \cos(\beta) + F_{grf} \cos(\theta)}{A} \quad (1)$$

145

146 and bending:

147

148 $$\sigma_b = \pm \frac{F_m \sin(\beta) - F_{grf} \sin(\theta) * h * y}{I}. \quad (2)$$

149

150 The muscle force F_m required to counteract the ground reaction force F_{grf} is defined as

151

152 $$F_m = \frac{F_{grf} * R}{r} \quad (3)$$

153

154 where r is the moment arm of F_m and R is the moment arm of F_{grf}; β is the angle of F_m to the
155 long axis of the bone; θ is the angle of F_{grf} to the long axis of the bone; and h $(= \frac{l}{2})$ is the height
156 to the bone's midshaft, where the bone's total length is l (Figure 2).

157 Moment arms were taken from empirical values for the metapodial-phalanx joint in
158 extant *Equus* (r = 30 mm and R = 100 mm for a 450 kg animal) [38,39] and scaled such that $r \propto$
159 $M_{body}^{0.43}$ [23,40], where M_{body} was the reconstructed body mass of each genus [33–36]. Effective
160 mechanical advantage (EMA), defined as $\frac{r}{R}$, scales $\propto M_{body}^{0.258}$. With a starting point of *Equus*
161 EMA = 30/100mm = 0.3, we scaled EMA and back-calculated R for all taxa. The ground
162 reaction force (F_{grf}) was set equal to a body-weight load for each species. In the first condition,
163 the whole load was placed on the centre metapodial. In the TRI condition, that load was reduced
164 proportional to TRI as discussed previously. We chose a β of 0° to reflect that the muscle-tendon
165 units act almost directly in line with the metapodials in extant horses [25,26].

166 Under a bending load, stress at the bone's midshaft cross-section will range from positive
167 (tensile side of the bend; anterior, if θ is positive) to negative (compressive side of the bend;
168 posterior, if θ is positive). We can therefore calculate the maximal stress on the anterior and
169 posterior surfaces as $\sigma_{AP} = \sigma_c \pm \sigma_b$, with axial compression reducing stress on the tensile
170 surface ($\sigma_c + \sigma_b$) and compounding stress on the compressive surface ($\sigma_c - \sigma_b$). Safety factor
171 was calculated as the ratio of the bone's fracture stress (approximately 200MPa in compression
172 and 170MPa in tension [41]) to the maximal stress calculated in this study. When a metacarpal
173 and metatarsal from the same specimen were available (n = 4), we assessed the ratio of maximal
174 stress in the metacarpal vs. metatarsal using the body-weight and TRI-scaled loading conditions.
175
176 **Results**
177 (a) Metapodial internal geometry
178 After phylogenetic correction, metapodial *A* (resistance to axial compression) shows
179 strong positive allometry (Figure 2A, Table S3). Metapodial I_{ML} (resistance to bending in the
180 anteroposterior direction) also shows strong phylogenetically corrected positive allometry
181 (Figure 2B, Table S4). For each metapodial specimen, cross-sectional geometry variables remain
182 consistent along the length of the bone with a typical peak near the articular ends (Figures 2C,
183 S2, S3). As TRI decreases in fossil equids, size-independent resistance to anteroposterior
184 bending increases, as shown by the higher values of size-corrected I_{ML} for lines of warmer colour
185 (Figure 2C). *Tapirus*, the outgroup, has significantly greater resistance to bending relative to
186 equids with similar TRI values. *Equus* metacarpals show the greatest size-independent resistance
187 to bending, followed by *Pliohippus* and the hipparionine horses. The lowest size-independent
188 resistance to bending is *Hyracotherium*. Results are similar for resistance to mediolateral

bending (Figure S2B), with higher overall values of *I*, reflecting the slight anteroposterior cross-sectional flattening of most metapodials in this study (see Figure 1).

(b) Metacarpal stress during normal (trotting) locomotion

During normal locomotion, the posterior metapodial surface experiences the greatest load due to the combination of bending and axial compression (Figure S4). The metacarpals in all taxa studied maintained a safety factor of at least 1.7, even without accounting for the side digits bearing some of the load (mean safety factor 3.1 ± 1.1; Table 1). The average posterior surface stress during normal locomotion supporting a body weight load is -70.1 ± 21.1MPa, higher than would be expected for trotting locomotion [25]. After scaling the load by TRI to account for side digits distributing the load, the average posterior surface stress is reduced to -31.6 ± 7.4MPa, yielding a higher and more consistent safety factor (6.7 ± 1.6) across taxa.

(b) Metacarpal stress during performance (acceleration/jumping) locomotion

During performance locomotion (Figure 3), the anterior metacarpal surface is loaded in tension and the posterior surface loaded in compression. Without scaling for TRI, many fossil taxa approach or surpass the tensile fracture stress of bone on the anterior surface and/or the compressive fracture stress on the posterior surface (black bars). Most tridactyl taxa exhibit posterior surface stresses within approximately 50MPa of fracture stress. The exceptions are the later, hipparionine horses (especially *Pseudhipparion* and *Cormohipparion*), as well as *Pliohippus* and *Equus*, which all exhibit stresses closer to -100MPa (a safety factor of 2). When accounting for the side digits by scaling the load relative to TRI, maximal stress is below -100MPa for almost all taxa (maximum -109MPa for one specimen of *Mesohippus,* a safety factor

of 1.8). Average posterior surface stress is -67.7 ± 19.5MPa, providing a safety factor of 3.2 ± 0.9. On the anterior surface, tensile stress averages 29.6 ± 14.2MPa for all taxa. In all cases, adjusting for TRI leaves maximal stresses within or below the safety factor range of 2-4 found in living animals [42].

(c) Metacarpal vs. metatarsal maximal stress

In *Mesohippus*, *Equus*, and extant *Tapirus*, metatarsal stresses range from 7 to 33% higher than metacarpal stresses under performance conditions with weight scaled by TRI (up to 25.5MPa difference; Table 2). In *Archaeohippus*, metatarsal stress is 8% higher than metacarpal stress (a 3.2MPa difference). Results are similar for a non-scaled load, but with higher magnitudes. Overall, results for all metatarsals follow the same pattern as metacarpals, with similar safety factors (Figure S5).

Discussion

(a) Simulated stress matches in vivo stress in *Equus*

Results for a Pleistocene fossil *Equus*, with maximal metacarpal stresses of -34MPa for normal trotting locomotion and -70MPa for performance locomotion, are similar to maximal in vivo stress from living *Equus* (-31MPa during forward locomotion and -53MPa for jumping [25]). After reducing the forces on the metacarpal relative to side digit proportions, mean safety factor during performance locomotion for all taxa (3.2±0.9) aligns closely with experimentally determined values of safety factors from 2 to 4 across a wide range of mammalian species [40,42]. Furthermore, *Mesohippus* and *Equus* metacarpal stresses agree with those calculated by Thomason (1985), who used more simplifying assumptions and less detailed 3D geometry but

incorporated estimates of foot posture (which we did not) [21]. During trotting locomotion with the side digits bearing proportional load, we calculate a posterior midshaft stress of -34MPa for *Equus* and -34MPa and -45MPa for two *Mesohippus* specimens in this study, which agrees with Thomason's results of -48.3MPa in *Equus* and -33.4MPa in *Mesohippus* [21].

(b) Stress on the centre metapodial decreases with increasing body mass

When a body-weight load is placed on MCIII, its midshaft stress decreases as body mass increases through evolutionary time (Figure 3, black bars). This result is in contrast with living vertebrates from mice to elephants, which show similar limb safety factor regardless of body mass [40]. Changes in internal geometry explain this pattern: resistance to bending and axial compression in the third metapodial shows strong positive allometry in the equid lineage (Figure 2A, 2B). Because cross-sectional area and second moment of area increased, total stress during locomotion is reduced as body mass increases. Not only is this pattern of safety factor unexpected, it suggests that many tridactyl taxa could not have safely loaded only metapodial III during high-performance locomotion (Figure 3, black bars). These results point to evolutionary compensation by the centre digit for increasing body mass and shrinking side digits, but also suggest that the side digits played a necessary role in earlier taxa. Postural changes in the angle of the metapodial to the ground reaction force could also influence safety factor as side digits were reduced and body mass increased. Although we do not account for postural changes in this study, less upright posture in earlier equids would likely increase the reconstructed stresses, as larger ground reaction force angles would lead to greater bending moments and larger muscle forces.

(c) Load-bearing side digits are critical in most tridactyl taxa

When side digits are load-bearing, metapodial midshaft stress remains approximately constant through equid evolution (white bars, Figure 3). Estimated metacarpal safety factor is biologically feasible and consistent (average safety factor of 3.2 ± 0.9). Even during more demanding locomotion such as acceleration or jumping, midshaft stress does not change with digit reduction or increasing body mass—consistent with bone stresses determined for extant quadrupeds [40].

We expected *Pliohippus* to have sufficient safety factor at high performance even without accounting for the side digits because the population of *Pliohippus pernix* from Ashfall, the source of our specimen, contains both tridactyl and monodactyl individuals [43]. Such variation would seem to suggest that the biomechanical role of the side digits for weight support, if any, was not critical during locomotion. Under the high-performance scenario, the *Pliohippus* metacarpal had a safety factor of 2 without side digits and 4 when scaling by TRI. These results bracket the *Equus* safety factor of 2.9 but are similar to the hipparionine horses, whose side digits probably did provide utility, as discussed in the next section. However, *Pliohippus* shows the highest size-independent resistance to anteroposterior bending after *Equus* and *Tapirus* (Figure 2). Our results do not definitively show that the side digits of *Pliohippus* at Ashfall were without weight support function, but support the possibility.

(d) Metacarpals resist bending slightly better than metatarsals

We hypothesized that the bending performance of metacarpals and metatarsals might be decoupled because of the asymmetrical nature of digit reduction between the forelimb and hind limb. With ground reaction force equivalent to one body-weight—which both the metacarpal and

281 metatarsal experience during faster locomotion in extant *Equus* [25,26]—and similar angle
282 deviations between bone and GRF alignment of 5° or 20°, the metatarsals of fossil horses
283 generally showed slightly higher stresses than the corresponding metacarpals from the same
284 specimens. These differences were small in magnitude, ranging from +11MPa to -3.2MPa in the
285 metatarsal relative to metacarpal (a maximum of 33% difference). Our results do not account for
286 a greater body weight load in the forelimb or a greater angle in the hind limb [26], which could
287 produce greater loads in the metacarpal or metatarsal respectively, but the values for both are
288 within experimental results for extant *Equus* [25,26]. We therefore do not find strong support for
289 evolutionary decoupling of the stresses experienced by the metacarpal and metatarsal.
290
291 (e) Evolutionary timing and the loss of functional side digits
292 Based on our results, side toes were critical for load-bearing to some extent through at
293 least *Parahippus,* the genus at the base of the grazing adaptive radiation. At that point in equid
294 evolution, the distal limb had been significantly elongated and the digits were reduced;
295 *Parahippus* had a TRI of 0.61, reduced from 0.89 in *Hyracotherium*. At that time, true grasslands
296 were part of the North American flora [44] and may have been spreading significantly [45],
297 which could have provided selective pressure for reduced distal limb mass to save on costs of
298 locomotion over large home ranges [15] or reduced the need for lateral stability [16]. Later, some
299 hipparionine horses (*Pseudhipparion* and *Cormohipparion*) evolved a centre metacarpal that may
300 have been robust enough to maintain an acceptable safety factor without load-bearing use of the
301 side digits (Figure 3, black bars). Although these genera show reasonable safety factors under the
302 conditions of our analysis, a trackway attributed to the closely related genus *Hipparion* shows
303 ground contact by the side digits [22], which would provide a greater safety factor for the centre

metacarpal (approximately 4 instead of 2). As Thomason [17] points out, the contact of side digits in the trackway also supports a possible stabilizing function for the side toes as argued by Shotwell [16]. Selection for stabilization could be separate from any need for stress reduction via load-bearing, and as such would be unrelated to safety factor in the traditional sense.

Conclusion

Our beam analysis indicates that fossil horse metapodials maintained a similar safety factor throughout evolution. Furthermore, as digits were reduced and body mass increased, the centre metapodial changed in its internal geometry, showing allometric increases in cross-sectional area and second moment of area relative to body size. According to our results, side digits were necessary for load-bearing in earlier taxa, including *Parahippus*, to avoid unsafe levels of stress in the centre metapodial. The mechanism of support could be directly through ground contact or, as has been suggested previously, indirectly via interdigital ligaments [17]. Our results support the hypothesis that increasing body mass was a potential driver of digit reduction because a single, robust digit could resist the increased bending forces better than three smaller digits of the same total bone area [14]. However, other factors were likely involved. In combination with increasingly parasagittal limb motion and lengthened distal limbs, the reduced side digits—with their reduced mechanical function—could have incurred sufficient inertial penalty to distal limb motions to either decrease speed or increase energetic cost [17,21]. Thus, selection may have been for a combination of increased strength and decreased inertia, or one followed by the other.

Supporting Data

All data, code, and results supporting this article are available on DataDryad [submission of manuscript to generate ID number]. The main results and supplemental methods have been uploaded as part of the supplementary material.

Competing Interests

We have no competing interests.

Author Contributions

All authors conceived and designed the study. BKM collected the data, wrote the code, analysed the data, and drafted the manuscript. All authors interpreted the data, edited the manuscript, and gave final approval for publication.

Acknowledgments

For assistance with collections access we thank J. Chupasko, J. Cundiff, M. Omura, M. Renczkowski, and C. Capobianco at the Harvard MCZ; J. Galkin and A. Gishlick at the AMNH; P. Holroyd at the UCMP; G. Corner and R. Secord at the UNSM; R. Otto at Ashfall Fossil Beds; and J. Head. J. MacLaren contributed TRI data. A. Parker assisted with data processing. We thank the Biewener and Pierce labs at Harvard for feedback on varying stages of this work.

Funding

Funding was provided by the Ashford Foundation, the Harvard Department of Organismic and Evolutionary Biology, and a Sigma Xi Grant in Aid of Research. BKM was supported by a NSF Graduate Research Fellowship (#DGE1144152) while this work was conducted.

References

1. Clifford AB. 2010 The evolution of the unguligrade manus in artiodactyls. *Journal of Vertebrate Paleontology* **30**, 1827–1839. (doi:10.1080/02724634.2010.521216)

2. Cooper WJ, Steppan SJ. 2010 Developmental constraint on the evolution of marsupial forelimb morphology. *Aust. J. Zool.* **58**, 1–15. (doi:10.1071/ZO09102)

3. De Bakker MAG, Fowler DA, Oude K den, Dondorp EM, Navas MCG, Horbanczuk JO, Sire J-Y, Szczerbińska D, Richardson MK. 2013 Digit loss in archosaur evolution and the interplay between selection and constraints. *Nature* **500**, 445–448. (doi:10.1038/nature12336)

4. Moore TY, Organ CL, Edwards SV, Biewener AA, Tabin CJ, Jenkins Jr. FA, Cooper KL. 2015 Multiple Phylogenetically Distinct Events Shaped the Evolution of Limb Skeletal Morphologies Associated with Bipedalism in the Jerboas. *Current Biology* **25**, 2785–2794. (doi:10.1016/j.cub.2015.09.037)

5. Saxena A, Towers M, Cooper KL. 2017 The origins, scaling and loss of tetrapod digits. *Phil. Trans. R. Soc. B* **372**, 20150482.

6. Young RL, Caputo V, Giovannotti M, Kohlsdorf T, Vargas AO, May GE, Wagner GP. 2009 Evolution of digit identity in the three-toed Italian skink *Chalcides chalcides*: a new case of digit identity frame shift. *Evolution & Development* **11**, 647–658. (doi:10.1111/j.1525-142X.2009.00372.x)

7. Coates MI, Clack JA. 1990 Polydactyly in the earliest known tetrapod limbs. *Nature* **347**, 66–69.

8. Cooper KL, Sears KE, Uygur A, Maier J, Baczkowski K-S, Brosnahan M, Antczak D, Skidmore JA, Tabin CJ. 2014 Patterning and post-patterning modes of evolutionary digit loss in mammals. *Nature* **511**, 41–45. (doi:10.1038/nature13496)

9. Lopez-Rios J *et al.* 2014 Attenuated sensing of SHH by Ptch1 underlies evolution of bovine limbs. *Nature* **511**, 46–51.

10. Cooper LN, Berta A, Dawson SD, Reidenberg JS. 2007 Evolution of hyperphalangy and digit reduction in the cetacean manus. *Anat Rec* **290**, 654–672. (doi:10.1002/ar.20532)

11. Shapiro MD, Shubin NH, Downs JP. 2007 Limb diversity and digit reduction in reptilian evolution. *Fins into limbs: evolution, development, and transformation* , 225–245.

12. Moore TY, Biewener AA. 2015 Outrun or Outmaneuver: Predator–Prey Interactions as a Model System for Integrating Biomechanical Studies in a Broader Ecological and Evolutionary Context. *Integr Comp Biol* **55**, 1188–1197. (doi:10.1093/icb/icv074)

13. MacFadden BJ. 1994 *Fossil Horses: Systematics, Paleobiology, and Evolution of the Family Equidae*. Cambridge University Press.

14. Simpson GG. 1951 *Horses: The Story of the Horse Family in the Modern World and through Sixty Million Years*. Oxford University Press.

15. Janis CM, Wilhelm PB. 1993 Were there mammalian pursuit predators in the Tertiary? Dances with wolf avatars. *Journal of Mammalian Evolution* **1**, 103–125.

16. Shotwell JA. 1961 Late Tertiary biogeography of horses in the northern Great Basin. *Journal of Paleontology* **35**, 203–217.

17. Thomason JJ. 1986 The functional morphology of the manus in the tridactyl equids *Merychippus* and *Mesohippus*: paleontological inferences from neontological models. *Journal of Vertebrate Paleontology* **6**, 143–161.

18. Biewener AA. 1998 Muscle-tendon stresses and elastic energy storage during locomotion in the horse. *Comparative Biochemistry and Physiology Part B: Biochemistry and Molecular Biology* **120**, 73–87.

19. Camp CL, Smith N. 1942 Phylogeny and functions of the digital ligaments of the horse. *Memoirs of the University of California* **3**, 69–124.

20. Sondaar PY. 1968 The osteology of the manus of fossil and recent Equidae, with special reference to phylogeny and function. *Verhandelingen der Koninklijke Nederlandse akademie van wetenschappen* **25**, 1–76.

21. Thomason JJ. 1985 Estimation of locomotory forces and stresses in the limb bones of recent and extinct equids. *Paleobiology* **11**, 209–220.

22. Renders E. 1984 The gait of *Hipparion* sp. from fossil footprints in Laetoli, Tanzania. *Nature* **308**, 179–181.

23. Biewener AA. 1990 Biomechanics of Mammalian Terrestrial Locomotion. *Science* **250**, 1097.

24. Rubin CT, Lanyon LE. 1984 Dynamic strain similarity in vertebrates; an alternative to allometric limb bone scaling. *Journal of theoretical biology* **107**, 321–327.

25. Biewener AA, Thomason J, Lanyon LE. 1983 Mechanics of locomotion and jumping in the forelimb of the horse (*Equus*): in vivo stress developed in the radius and metacarpus. *Journal of Zoology* **201**, 67–82.

26. Biewener AA, Thomason JJ, Lanyon LE. 1988 Mechanics of locomotion and jumping in the horse (*Equus*): in vivo stress in the tibia and metatarsus. *Journal of Zoology* **214**, 547–565. (doi:10.1111/j.1469-7998.1988.tb03759.x)

27. MacLaren JA, Nauwelaerts S. 2016 A three-dimensional morphometric analysis of upper forelimb morphology in the enigmatic tapir (Perissodactyla: *Tapirus*) hints at subtle variations in locomotor ecology. *Journal of Morphology* **277**, 1469–1485. (doi:10.1002/jmor.20588)

28. Doube M, Kłosowski MM, Arganda-Carreras I, Cordelières FP, Dougherty RP, Jackson JS, Schmid B, Hutchinson JR, Shefelbine SJ. 2010 BoneJ: Free and extensible bone image analysis in ImageJ. *Bone* **47**, 1076–1079. (doi:10.1016/j.bone.2010.08.023)

29. Schneider CA, Rasband WS, Eliceiri KW. 2012 NIH Image to ImageJ: 25 years of image analysis. *Nat Meth* **9**, 671–675. (doi:10.1038/nmeth.2089)

30. Cuff AR, Sparkes EL, Randau M, Pierce SE, Kitchener AC, Goswami A, Hutchinson JR. 2016 The scaling of postcranial muscles in cats (Felidae) II: hindlimb and lumbosacral muscles. *J. Anat.* **229**, 142–152. (doi:10.1111/joa.12474)

429 31. Warton DI, Duursma RA, Falster DS, Taskinen S. 2012 smatr 3–an R package for estimation
430 and inference about allometric lines. *Methods in Ecology and Evolution* **3**, 257–259.

431 32. Doube M, Yen SC, Kłosowski MM, Farke AA, Hutchinson JR, Shefelbine SJ. 2012 Whole-
432 bone scaling of the avian pelvic limb. *Journal of Anatomy* **221**, 21–29.

433 33. MacFadden BJ. 1986 Fossil horses from 'Eohippus'(*Hyracotherium*) to *Equus*: scaling,
434 Cope's Law, and the evolution of body size. *Paleobiology* **12**, 355–369.

435 34. Garland T, Janis CM. 1993 Does metatarsal/femur ratio predict maximal running speed in
436 cursorial mammals? *Journal of Zoology* **229**, 133–133.

437 35. Damuth J. 1990 Problems in estimating body masses of archaic ungulates using dental
438 measurements. *Body size in mammalian paleobiology: estimation and biological*
439 *implications* , 229–253.

440 36. Janis CM, Gordon IJ, Illius AW. 1994 Modelling equid/ruminant competition in the fossil
441 record. *Historical Biology* **8**, 15–29. (doi:10.1080/10292389409380469)

442 37. Rumph PF, Lander JE, Kincaid SA, Baird DK, Kammermann JR, Visco DM. 1994 Ground
443 reaction force profiles from force platform gait analyses of clinically normal mesomorphic
444 dogs at the trot. *American Journal of Veterinary Research* **55**, 756–761.

445 38. Brown NA, Pandy MG, Buford WL, Kawcak CE, McIlwraith CW. 2003 Moment arms about
446 the carpal and metacarpophalangeal joints for flexor and extensor muscles in equine
447 forelimbs. *American Journal of Veterinary Research* **64**, 351–357.

448 39. Bullimore SR, Burn JF. 2006 Dynamically similar locomotion in horses. *Journal of*
449 *Experimental Biology* **209**, 455–465. (doi:10.1242/jeb.02029)

450 40. Biewener AA. 1991 Musculoskeletal design in relation to body size. *Journal of*
451 *Biomechanics* **24**, 19–29. (doi:10.1016/0021-9290(91)90374-V)

452 41. Currey JD. 2014 *The mechanical adaptations of bones*. Princeton University Press.

453 42. Biewener AA. 1989 Scaling body support in mammals: limb posture and muscle mechanics.
454 *Science* **245**, 45–48.

455 43. Tucker ST, Otto RE, Joeckel RM, Voorhies MR. 2014 The geology and paleontology of
456 Ashfall Fossil Beds, a late Miocene (Clarendonian) mass-death assemblage, Antelope
457 County and adjacent Knox County, Nebraska, USA. *Field Guides* **36**, 1–22.

458 44. Strömberg CA. 2011 Evolution of grasses and grassland ecosystems. *Annual Review of Earth*
459 *and Planetary Sciences* **39**, 517–544.

460 45. Retallack GJ. 2007 Cenozoic paleoclimate on land in North America. *The Journal of*
461 *Geology* **115**, 271–294.

462

463

Figure Captions

Figure 1. Toe Reduction Index (TRI) shown for the genera sampled in this study. Values range from 0 (red; no side toes) to 1 (dark blue; all digits of equal size). Note the continuous variation captured in tridactyl genera (i.e., all genera except *Tapirus*, *Hyracotherium*, and *Equus*), which is ignored by discrete categories of digit state. Midshaft cross-section of MCIII shown on the right, except for *Anchitherium*, for which we had only MTIII. Cross-sections are scaled to the same approximate size.

Figure 2. A) Scaling relationship of log-transformed and phylogenetically corrected body mass vs. cross-sectional area (solid blue line), with 95% confidence interval of the slope in grey. Black dashed line shows the null hypothesis of isometry. B) The same as in 2A, but for second moment of area about the mediolateral axis (i.e., resistance to anteroposterior bending). C) Size-corrected second moment of area about the mediolateral axis (I_{MLnorm}) vs. position on metacarpal III normalized by total length, showing size-independent resistance to bending in the anteroposterior direction. Each line is a genus, coloured by its TRI value from Figure 1. Lines are smoothed to account for cracks in fossil specimens.

Figure 3. Midshaft metacarpal III stresses during performance locomotion ($\theta = 20°$), with body-weight (black bars) and TRI-scaled (white bars) load. Genus average stresses are shown at anterior (top panel) and posterior surfaces (bottom panel) of the bone, where bending forces are maximized. Absolute values are graphed, but sign is indicated on the y-axis and loading is labelled as compressive or tensile. Approximate fracture stress of bone shown by a dashed red

line. The range of limb bone safety factors found in living mammals is shown as a light blue panel [42]. Coloured bars represent TRI value for each genus from Figure 1.

Table Captions

Table 1. Safety factors for differing loads and locomotion types.

Table 2. Same-specimen metacarpal vs. metatarsal stress differences (posterior surface), shown both for normal (trotting) and performance (acceleration/jumping) locomotion. Values used are from TRI-scaled trials. Difference is $\sigma\mathrm{MCIII} - \sigma\mathrm{MTIII}$, so positive values indicate higher stress in the metatarsal. Percent difference is $-\left(\frac{\mathrm{difference}}{\sigma\mathrm{MCIII}}\right) * 100$.

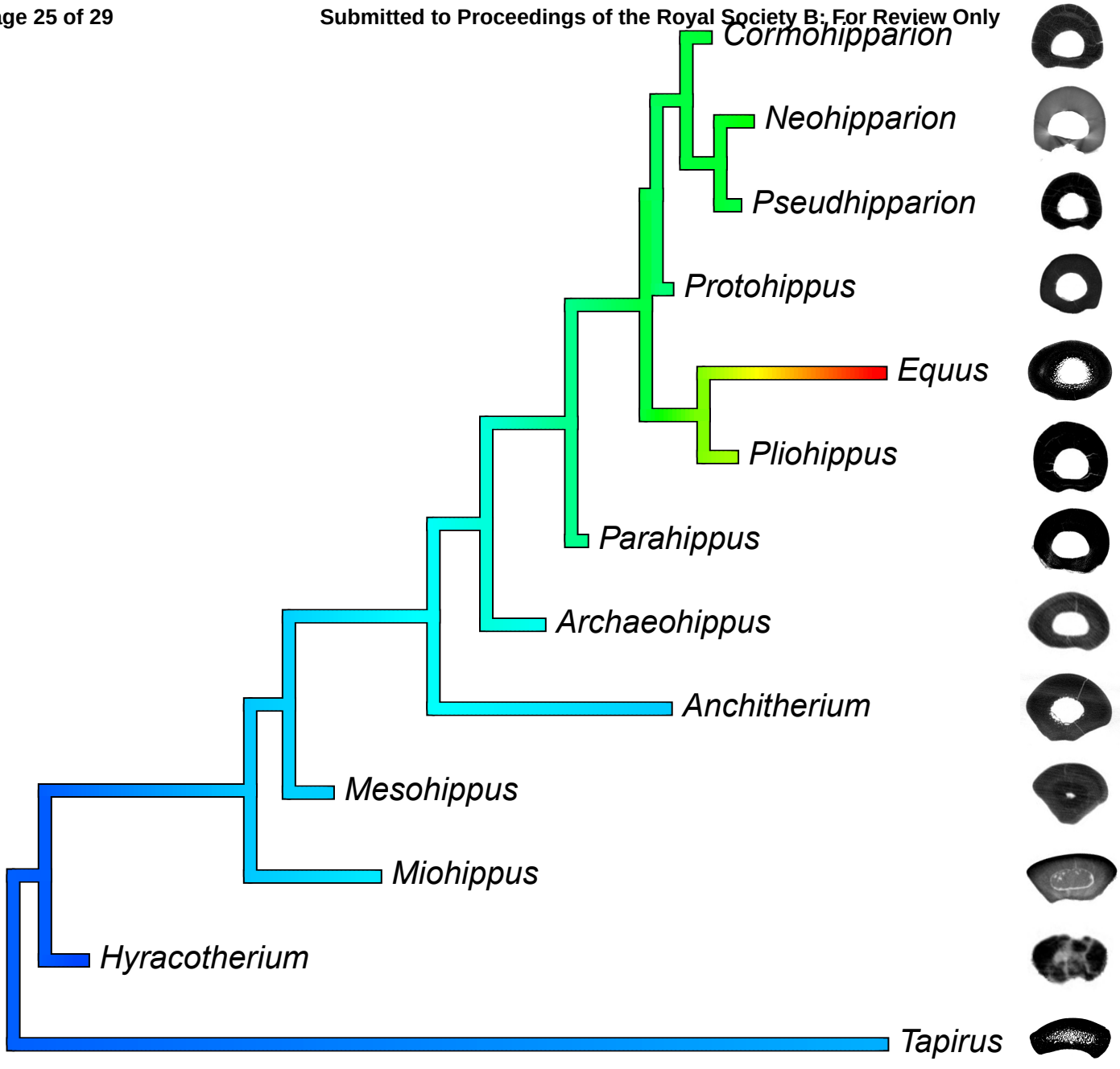
Cormohipparion
Neohipparion
Pseudhipparion
Protohippus
Equus
Pliohippus
Parahippus
Archaeohippus
Anchitherium
Mesohippus
Miohippus
Hyracotherium
Tapirus
0
Toe Reduction Index
1

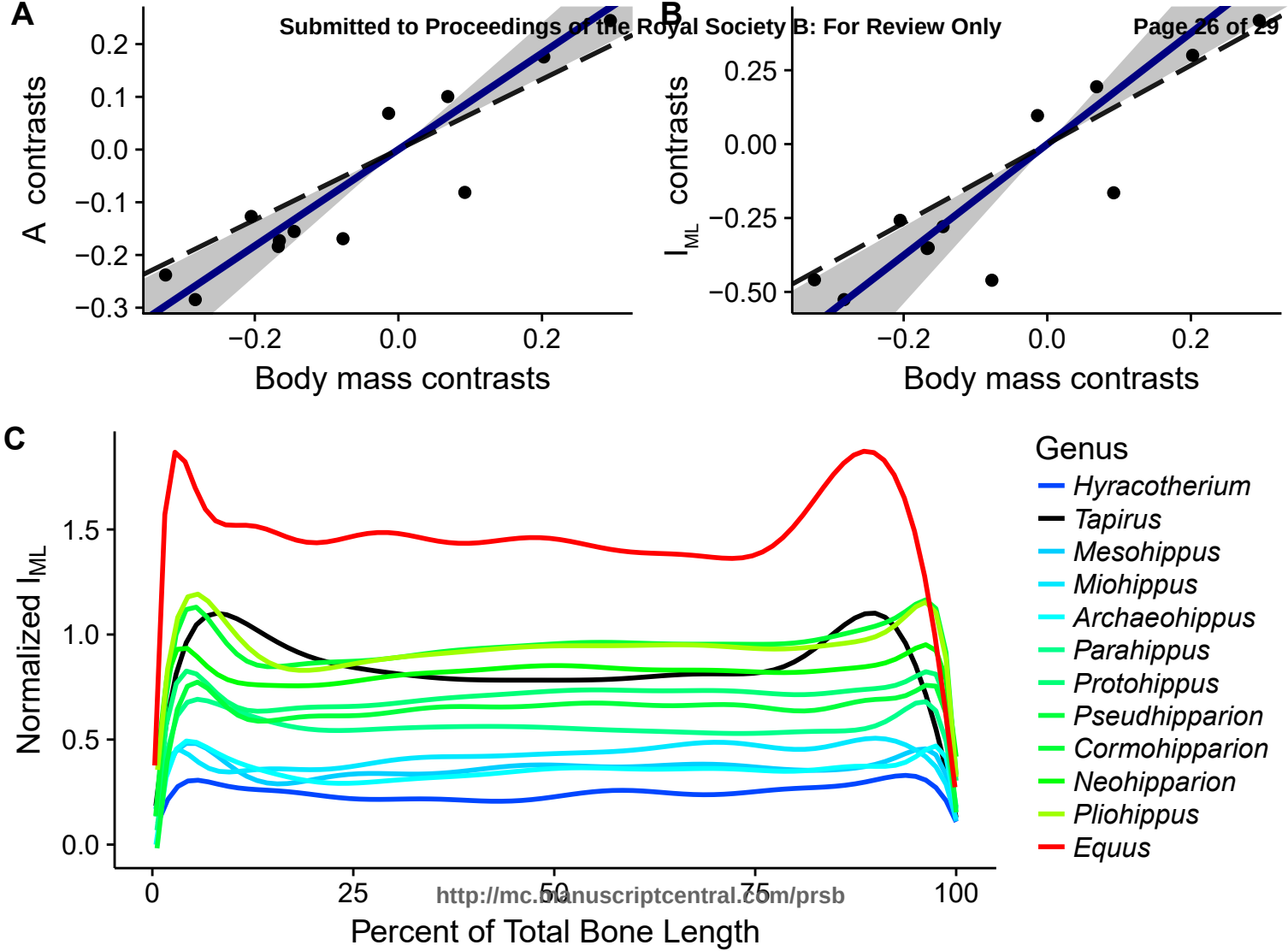

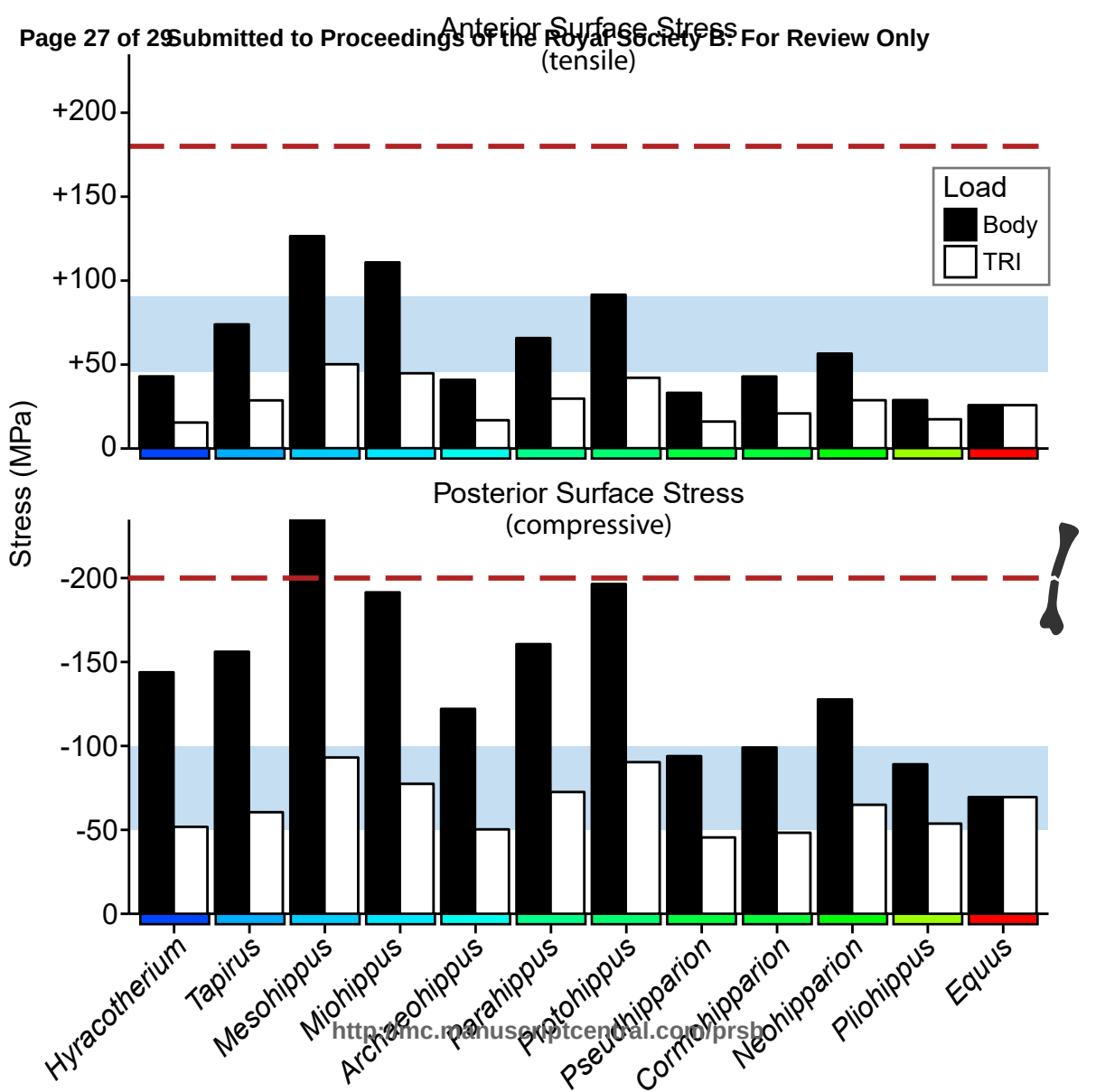

Table 1.

Condition	Scenario	Safety Factor			
		Mean	SD	Min	Max
Body	Normal (Trotting)	3.1	±1.1	1.7	5.8
Body	Performance	1.5	±0.6	0.7	2.9
TRI	Normal (Trotting)	6.7	±1.6	4.4	10
TRI	Performance	3.2	±0.9	1.8	5

Table 2.

Specimen No.	**Genus**	**Scenario**	**σ MCIII** (MPa)	**σ MTIII** (MPa)	**Difference** (MPa)	**% Difference**
MCZ13478	*Equus*	Normal	-34.3	-39.7	5.4	15.7
MCZ63107	*Tapirus*	Normal	-27.5	-28.7	1.2	4.4
MCZ6927	*Mesohippus*	Normal	-34.3	-42.5	8.2	23.9
MCZ7283	*Archaeohippus*	Normal	-20.1	-19.7	-0.4	-2.0
MCZ13478	*Equus*	Performance	-69.5	-80.5	11.0	15.8
MCZ63107	*Tapirus*	Performance	-60.5	-64.7	4.2	6.9
MCZ6927	*Mesohippus*	Performance	-77.2	-102.7	25.5	33.0
MCZ7283	*Archaeohippus*	Performance	-40.1	-36.9	-3.2	-8.0